On the interest of using full field measurements in ductile damage model calibration

Emile Roux, Pierre-Olivier Bouchard

International Journal of Solids and Structures 72 (2015) 50–62

Contents lists available at ScienceDirect

International Journal of Solids and Structures

journal homepage: www.elsevier.com/locate/ijsolstr

On the interest of using full field measurements in ductile damage model calibration

E. Roux [a,*], P.-O. Bouchard [b]

[a] Université de Toulouse, Institut Supérieur de l'Aéronautique et de l'Espace (ISAE), Institut Clément Ader (ICA EA 814), Toulouse, France
[b] MINES ParisTech, PSL – Research University, CEMEF – Centre de mise en forme des matériaux, CNRS UMR 7635, CS10207 rue Claude Daunesse, 06904 Sophia Antipolis Cedex, France

ARTICLE INFO

Article history:
Received 28 July 2014
Received in revised form 12 June 2015
Available online 21 July 2015

Keywords:
Ductile damage model
Parameter identification
Inverse analysis
Full field measurements

ABSTRACT

This paper is focused on the identification method by inverse analysis of ductile damage model parameters. The Lemaitre damage model is considered. The aim is to assess the interest of using local measurements, such as full field measurements, in the calibration process. Basic approach using only load-displacement measurements from a tensile test is first described and discussed. Secondly necking measurements are added in the calibration process. And finally an inverse analysis approach including full field measurements in a large deformation framework is presented. For each step particular attention is paid to the definition of the objective function to catch efficiently the softening behavior and the fracture of the sample. This step-by-step approach allows understanding the lack of information embedded in the load-displacement curve to calibrate such a model. It also highlights the multi-extrema aspect of the optimization problem. The introduction of local measurements, as necking and even more as displacement fields, is an efficient way of overcoming this lack of information. The analysis is based on kriging response-surfaces built during the minimization of the objective function. These surfaces highlight the weak sensitivity of one of the Lemaitre model parameters (the *b* parameter) when only the load-displacement curve is taken into account. The sensitivity is then improved when local measurements are considered. The use of local measurement also leads to the removal of correlation between model parameters.

1. Introduction

Nowadays the prediction of ductile damage in manufacturing processes is essential to avoid any failure during the forming stage and to improve final industrial components mechanical strength. This requires both a good understanding of the process itself and the use of accurate material behavior law for a finite element analysis of the process (Bouchard et al., 2008; Roux and Bouchard, 2013). Ductile damage is strongly linked with the plastic behavior of the material, and failure occurs along with the combined mechanisms of plastic strain localization (diffuse and localized necking) and damage nucleation, growth and coalescence. Many studies related to necking phenomena for tensile specimen can be found in the literature (Bridgman, 1944; Chen, 1971) and more recently the works of (Tardif and Kyriakides, 2012; Kim et al., 2013) can be cited. Moreover many ductile damage models are available in the literature (Gurson, 1977; Lemaitre and Desmorat, 2005; Rousselier, 1987; Tvergaard and Needleman, 1984). However the accuracy of these models directly relies on the accuracy of the identification of its parameters for each material.

The damage model parameters need to be identified before being used in any finite element software. This calibration stage is essential and is not taken into account seriously enough when comparing different ductile damage models or fracture criteria. In the end, when a model does not give good results, it is difficult to state whether this is due to the damage model itself or to a bad parameters identification stage. The aim of this paper is to illustrate the difficulty of identifying such damage parameters and the importance of accounting for local observables in addition to global observables. In addition, damage models are known to be mesh sensitive and therefore the mesh size is an important parameter to take into account for relevant calibration results. This dependency is strong for classical coupled damage models and is weaker (but non negligible) when non-local models are used (El Khaoulani and Bouchard 2013). Therefore in this work a fixed mesh is used to overcome this mesh dependency issue and concentrate on the influence of local observables on the enrichment of the calibration process.

* Corresponding author. Tel.: +33 (0)5 61 17 11 96.
E-mail address: emile.roux@isae.fr (E. Roux).

http://dx.doi.org/10.1016/j.ijsolstr.2015.07.011
0020-7683/

Several works focusing on damage parameters identification can be found in the literature. These works are dealing with different damage models, but some general remarks can be formulated.

Fratini et al. (1996) reported an inverse analysis procedure to identify the parameters of a ductile damage model. The identification was based on the load-displacement curve of a tensile test. One of the major conclusions of this paper was that the optimization problem had multiple minima. And it is also interesting to notice that necking measurements were used as validation. Then Mahnken (2002) presented a calibration method where necking measurements were added as observable. Both load-displacement curve and necking evolution were used to compute the objective function, a weighted sum was used to overcome the dimensional issue between load and necking reduction. This work was applied to the Gurson damage model and to the Rousselier damage model. Munoz-Rojas et al. (2010) also reported a calibration method of the Gurson damage model using both force and necking measurements. In this work the focus was made on the minimization method. Genetic optimization method was used to tackle the issue of the non-uniqueness of the solution. Broggiato et al. (2007) measured the full necking profile of the sample to identify the parameters of the GTN model. Identification results obtained with the load-displacement curve coming from three tensile tests with different notch radii were compared with the identification results coming from one test, but where both load-displacement curve and necking profile were used. The richness of the necking profile allows obtaining the same accuracy. Springmann and Kuna (2006) enriched the calibration procedure with displacement field measurements to identify the parameters of the GTN damage model and the parameters of an extended Rousselier damage model.

The purpose of full field measurements is to have a better description of the stain localization. Multiple minima issues were reported by the authors even though local measurements were taken into account. Abbassi et al. (2013) also performed calibration of the GTN model using displacement field measurements coupled to a neural network algorithm. Using full field measurements is a very promising way to improve the efficiency of the calibration method. Full field measurement approaches are well established for brittle material (Bouterf et al., 2014; Périé et al., 2009). These works were based on the analyses of complex mechanical tests (bending test and biaxial tension test), and the richness of the observable led to an accurate calibration damage model. In order to use these powerful approaches in ductile damage model calibration, a step further must be done in order to take into account large deformations. Another family of damage model must also be mentioned, the uncoupled damage model like the Bai and Wierzbicki's model (Bai and Wierzbicki, 2008); calibration of such model is address by Cao et al. (2013). In the work of Cao et al. multiple tests were performed under different stress states to identify the fracture locus.

According to the published works it is now establish that the load-displacement curve of one single tensile test is not rich enough to identify in a unique way the parameters of a ductile damage model. This uniqueness issue is due on the one hand to the high number of parameters to identify, and on the other hand to the coupled effect of necking and damage growth on the softening behavior. Two options are available to overcome this uniqueness issue:

- Multiple tests can be used in order to vary the stress state (stress triaxiality ratio and Lode angle). And then all the measured load-displacement curves are gathered in an inverse analysis procedure. This approach is called the classical approach in Broggiato et al. (2007). An example of this approach can be found in Guo et al. (2013).
- Many complementary information can be extracted from one test by using full filed measurement method in order to calibrate the model with a unique test.

In this paper, the authors made the choice of analyzing all the information that can be extracted form one simple tensile test. The goal of this paper is to show the importance of accounting for local measurements if one wants to obtain a unique set of values in the identification of hardening and damage parameters. In addition, the use of response surfaces helps understanding non-uniqueness problem as well as correlation between parameters issue.

In this work a calibration methodology based on a tensile test is built up. For simplicity reasons, a single test is used here to illustrate the methodology. However this approach can be easily extended to multiple mechanical tests. Three kinds of measurements are taken into account in the calibration method: the load-displacement curve, the necking evolution curve, and displacement full field measurements on one side of the sample. In Section 2 the Lemaitre damage model and finite element framework are presented. In Section 3, the global framework of the calibration by inverse analysis is described. In the following sections the interest of using richer measurements is demonstrated step by step. In Section 4, the results obtained with a simple load-displacement curve are shown and discussed. Special attention is paid to the definition of the cost function. In Section 4, the necking measurement is added to the calibration method, and finally Section 5 demonstrates the interest of using full field measurements in the identification of ductile damage parameters. For each section, response surfaces will be used to show local and global minima regarding the minimization of the cost function.

In order to concentrate on the efficiency and the accuracy (or inaccuracy!) of the calibration method, the choice was made by the authors to work only in a numerical framework. This means that the experimental measurements are not coming from a real experimental test but that they are generated using a finite element simulation. The main advantage of this choice are on the one hand to avoid uncertainty related to the plastic behavior of the material, the focus is therefore only on the damage model, and on the other hand to avoid any numerical sensitivity such as mesh size dependency. In addition, with this approach, the exact solution is known!

2. The Lemaitre damage model

In this work an extended version of the Lemaitre damage model (Lemaitre, 1992) is used. This model, enhanced by Bouchard et al. (2011), takes into account more complex loading paths.

The constitutive law is based on the additive decomposition of a strain increment into an elastic part and a plastic part. The elastic part is described by an isotropic elastic law. The plastic part is described by a von Mises criterion with an isotropic hardening, which is described by the following rule:

$$\sigma_0 = \sigma_y + K\bar{\varepsilon}^n \tag{1}$$

where σ_0 is the flow stress, σ_y is the initial yield stress, K the material's consistency, $\bar{\varepsilon}$ the equivalent plastic strain, and n is the hardening exponent.

The evolution law of the Lemaitre ductile damage model (Bouchard et al., 2011) is given here:

$$\dot{w} = \begin{cases} \frac{\dot{\lambda}_{pl}}{1-w}\left(-\frac{Y}{S_0}\right)^b & \text{if } 0 \leqslant T_x \quad \text{and} \quad \text{if } \bar{\varepsilon} > \bar{\varepsilon}_d \\ \frac{\dot{\lambda}_{pl}}{1-hw}\left(-\frac{Y}{S_0}\right)^b & \text{if } -1/3 \leqslant T_x < 0 \quad \text{and} \quad \text{if } \bar{\varepsilon} > \bar{\varepsilon}_d \\ 0 \quad \text{if } T_x < -1/3 \quad \textit{or} \quad \text{if } \bar{\varepsilon} > \bar{\varepsilon}_d \\ 0 \quad \text{and} \quad w = 1 \quad \text{if } w \geqslant w_c \end{cases} \tag{2}$$

where w is the damage parameter, $\bar{\varepsilon}_d$ is the plastic strain threshold for damage growth, λ_{pl} is the plastic multiplier, $T_x = -p/\sigma_{eq}$ is the stress triaxiality ratio (σ_{eq} is the equivalent von Mises stress, and p the hydrostatic pressure).

$Y = \frac{-\sigma_{eq}^2}{2E(1-w)^2}\left[\frac{2}{3}(1+\upsilon)+3(1-2\upsilon)\,T_x^2\right]$ corresponds to the strain energy release rate (E and υ are respectively the Young modulus and the Poisson ratio), S_0 and b are material damage parameters, and h is the void closure effect parameter (Ladevèze and Lamaitre, 1984). When w is equal to zero, the material is undamaged. And when w tends towards 1, the material is fully damaged.

The Lemaitre damage model described in (Eq. (2)) is implemented in the Cimlib library (El Khaoulani and Bouchard, 2012). The damage evolution is coupled to an elastic plastic behavior. The coupling between the material behavior and the damage evolution is done using the concept of effective stress $\tilde{\sigma}$ (Lemaitre, 1992):

$$\tilde{\sigma} = \sigma/(1-w), \tag{3}$$

where σ is the stress tensor.

The definition of this effective stress induces the coupling with the elastic and with the plastic part of the behavior law (Eq. (1)). A weak coupling is used in this work. For an analysis of the influence of damage coupling on numerical results, the reader can refer to El Khaoulani and Bouchard (2013).

This constitutive behavior is implemented using an updated lagrangian formulation and large plastic strains are considered. A mixed velocity–pressure formulation with a 3D enhanced ($P1^+/P1$) element is used. A simple one step Euler scheme is used for the time integration. Therefore this incremental formulation remains valid if the time step is small enough. This mixed formulation is well adapted to solve incompressible or quasi incompressible flow as elastic-plastic problem. For more details about the constitutive modeling, the reader can refer to Wagoner and Chenot (2001) for the general framework and to Bouchard et al. (2011) and El Khaoulani and Bouchard (2013) for the damage model implementation in the mixed velocity-pressure formulation.

3. Calibration procedure using inverse analysis approach

Due to the non-linearity of the problem and the coupling between material behavior and damage an inverse analysis approach is needed to calibrate the damage model. In fact direct fitting approaches cannot be used here; the non-linearity of the model itself and the non-linearity due the structural effect of the tensile test (necking) make the computation of a stress-strain curve difficult; this stress-strain curve is needed in direct fitting approaches. Based on the work of Bridgman (1944) and Chen (1971) tensile test results can be interpreted as strain-stress curves assuming the necking phenomena. The proposed approach here is described on the basis of a simple tensile test, but the final aim is to apply the same methodology on more complex tests. Examples of calibration of elasto-plastic models based on complex tests can be found in the literature (Kim et al., 2014; Pottier et al., 2012).

The main idea of inverse approaches is to fit numerical results coming from a FE simulation on experimental data. This fitting is done iteratively by tuning the material parameters values in the model in order to minimize a cost function. The gap between the numerical results (*FEres*) and experimental observable (*Obs*) is computed thanks to the objective function $fc(P)$:

$$fc(P) = |FEres(P) - Obs| \tag{4}$$

where P is the set of material parameters values, and $|\ldots|$ is a generic formulation to compute the gap between both measurements. An explicit formulation of this function is given in the following sections. Once this objective function is defined, a minimization method is needed to reduce the gap between *FEres* and *Obs*. This minimization procedure finally leads to find the parameter values P which represent the behavior of the material.

$$P = \arg\min_{\tilde{P}\in X}(fc(\tilde{P})) \tag{5}$$

where X is the research space of the material parameters P.

To achieve this calibration by inverse analysis the key points are:

- one or several mechanical tests,
- a numerical model of the mechanical tests,
- observables that can be compared between the mechanical test and the numerical model,
- an explicit formulation of the objective function,
- a minimization method.

The observables and the objective function are described in the following sections, while the mechanical test, its FE model and the minimization method are described in this section.

3.1. The mechanical test and its FE model

The tensile test used here is a normalized test (NF EN 10002-1). The dimensions of the sample are given in Fig. 1, the thickness of the sample is 1 mm. The reader must keep in mind that experimental results are replaced here by simulation results with a well-known set of hardening and damage parameters; therefore the mechanical test and the model are formally identical. The results obtained with this 3D simulation will be called "digital experimental data" in the following.

The digital experimental data are generated using the described model, and the nominal value of each parameter can be found in Table 1. The FE model (Fig. 1b) is a full 3D model using 3D enhanced tetrahedral ($P1^+/P1$) element as described in Section 2. Two symmetry planes are defined: the first one is normal to the z axis and the second is normal to the x axis. The left side of the sample is fully clamped, while on the right side a constant velocity in the tensile direction is applied. The mesh size is set to 1.5 mm outside of the necking area, and a refinement of a factor 10 is applied within the center area of the sample. This refinement allows improving the accuracy of the results, but the reader must keep in mind that results are strongly mesh dependent. The use of digital experimental data (with always the same mesh) is a way to avoid this dependency and to concentrate on model sensitivity itself. Using a sufficiently fine mesh has been shown to be important to describe necking (diffuse and localized necking) accurately (Dunand and Mohr, 2010; Tardif and Kyriakides, 2012).

3.2. The minimization method

In order to solve the minimization problem (Eq. (5)) a minimization algorithm is necessary. According to the specificity of this optimization problem the choice is made to use a meta-model based algorithm. In fact the evaluation of the objective function linked to one set of parameters P requires a non-linear FE computation, and this simulation is time consuming. Therefore the number of objective function evaluations must be kept low in order to obtain results in a reasonable time. Meta-model based algorithms are an efficient way to overcome this expensive simulation issues. Moreover, the optimization problem exhibits a multi-modal behavior, multiple minima are observed in calibration of ductile damage model (Munoz-Rojas et al., 2010). Therefore the optimization method should be a global optimization method. The authors have made the choice of working with the Efficient Global

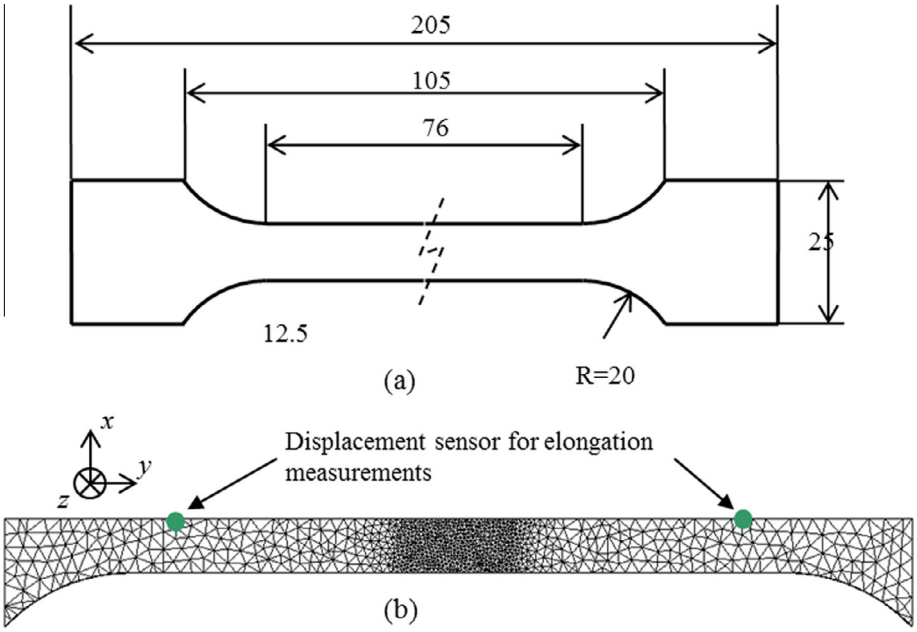

Fig. 1. (a) Normalized tensile test sample (dimension in mm), (b) FE mesh of the tensile test.

Table 1
Nominal parameter values used to generate the digital experimental data.

Parameters	Value	Description
E	69	Young modulus [GPa]
v	0.3	Poisson ration [–]
σ_y	46	Yield stress [MPa]
K	430	Material's consistency [MPa]
n	0.34	Hardening exponent [–]
b	1	Damage parameter [–]
S_0	0.7	Damage parameter [MPa]
w_c	0.8	Critical damage value [–]
$\bar{\varepsilon}_d$	0.16	Plastic strain threshold for damage growth [–]
h	0.2	Void closure effect parameter [–]

Optimization (*EGO*) algorithm developed initially by Jones et al. (1998). This algorithm has shown to have a good behavior in the field of forming process optimization involving ductile damage (Roux and Bouchard, 2013).

The *EGO* algorithm is a global optimization algorithm based on sequential enrichment of a kriging meta-model. The main steps of this algorithm are described in Algorithm 1. This procedure allows finding a minimum of the objective function *fc*. Moreover the parallel extension of the enrichment method which is described in Ginsbourger et al. (2010) is suitable to solve time consuming problems.

The choice is made to map the objective function all over the design space with a meta-model. This map is then used to explore the design space and to find the minimum area. The two key points of this algorithm are the kriging meta-model (Algorithm 1, line 5) and the way to exploit this meta-model by maximization of the Expected Improvement (Algorithm 1, line 6) criterion. More details about the minimization method and the kriging meta-model can be found in Jones et al. (1998) and Roux and Bouchard, (2013).

One of the advantages of the algorithm is to build a meta-model during the minimization process. This meta-model maps the objective function and is therefore a powerful tool to analyze the correlation between parameters and the sensitivity of the parameters on the objective function. In fact the meta-model is an approximation of the objective function all over the design space; therefore it can be used to analyze the evolution of the objective function all over the design space. These "landscape" plots are particularly useful to detect multiple extrema, weak sensitivity issues or correlation between parameters.

Algorithm 1: Global optimization method (Jones et al., 1998)

1:	$i = 1$	
2:	DBp= init()	// DBp is the database of parameter set, $DBp \in X$
3:	$DBy = fc(DBp)$	// "black box" function call DBy is the database of objective function values associated to DBp.
4:	While (i<imax) do	
5:	Meta = MetaModeling(DBp,DBy)	// meta-model generation and calibration
6:	$newDBp$ =argmin(Meta)	// exploration and exploitation using the expected improvement criterion
7:	DBp =[$DBp \cup newDBp$]	// data enrichment
8:	DBy=[$DBy \cup fc(newDBp)$]	// "black box" function call
9:	i=i+1	
10:	end	

4. Calibration based on a global measurement: the load-displacement curve

The first choice, which is often made in the literature (Abbasi et al., 2011; Fratini et al., 1996), is to use classical data coming from tensile test: the load-displacement curve. Guo et al. (2013) also used load-displacement curves coming from tensile and shearing tests to identify the Rousselier damage model parameters.

4.1. Objective function based on load-displacement curves including softening and fracture of the sample

The displacement is measured thanks to an extensometer, and the force is the reaction force measured at the jaws of the tensile setup. This kind of measurements allows obtaining 2-dimensional curves. On theses curves, one can observe the common stages of a tensile test: elasticity, hardening, softening and fracture. The objective function is defined to evaluate the gap between the measurements coming from the experiments and from the numerical model.

A classical square sum formulation is usually used to compute the difference between numerical and experimental results. A generic form can be found in (Eq. (6)). In order to make this formulation non-sensitive to the sampling rate, an integral form is used. This formulation is given in a continuous form in (Eq. (7)) while the same formulation is expressed in a discrete form in (Eq. (8)).

$$f_F(P) = \sum_{i=1}^{n} \left(Obs_i^{num}(P) - Obs_i^{\exp}\right)^2 \tag{6}$$

$$f_F(P) = \sqrt{\frac{\int_x \left(Obs^{num}(P,x) - Obs^{\exp}(x)\right)^2 dx}{\min\left(\int_x \left(Obs^{\exp}(x)\right)^2 dx, \int_x \left(Obs^{num}(P,x)\right)^2 dx\right)}} \tag{7}$$

$$\begin{cases} f_F(P) = \sqrt{\dfrac{\sum_{i=1}^{n} \left(Obs_i^{num}(P) - Obs_i^{\exp}\right)^2 \Delta x_i}{\min\left(\sum_{i=1}^{n} \left(Obs_i^{\exp}\right)^2 \Delta x_i, \sum_{i=1}^{n} \left(Obs_i^{num}(P)\right)^2 \Delta x_i\right)}} \\ \Delta x_i = x_i - x_{i-1} \end{cases} \tag{8}$$

where n is the number of measurement points, Obs_i^{num} and $Obs_i^{\exp}$ are the measured loads, and x_i its associate displacement. Most of the time, the measurements Obs^{num} and $Obs^{\exp}$ are sampled with non-coincident x values; therefore an interpolation must be done to express the measurement on the same x basis. In practice the measurements with the lower sampling rate are interpolated on the displacement coming from measurements with the higher sampling rate.

This formulation is therefore non-sensitive to the sampling rate since the use of the integral based formulation makes the objective function independent from the number and the rate of measurement points. The formulation can be useful when an adaptive time stepping scheme is adopted in the simulation or when a variable sampling rate is used to record the load-displacement curve.

In order to concentrate on damage evolution the focus must be made on the last part of the curve: from hardening to fracture. During the calibration process several set of material parameters are tested; all of them leads to different mechanical behavior and therefore to a different fracture point. This mechanical behavior differs also from the experimental measurement. For example it can occur that the numerical sample exhibits a fracture point at a lower displacement than the one from the experimental sample (Fig. 2a). Therefore there is a displacement range in-between the facture points of the numerical sample and the one of the experimental sample where only one load measurement is available (Fig. 2a, gray area in the load-displacement graph). Therefore a specific treatment must be applied to catch efficiently this part of the curve.

Several computations of the cost function were considered to find a relevant way of accounting for the fracture point in the objective function. Three strategies are presented here. For all of them the objective function is evaluated for 121 sets of parameters (S_0, $\bar{\varepsilon}_d$). These 121 sets of parameters are sampled using a regular grid centered on the nominal values. The obtained evolution of the objective function is shown in Fig. 2.

The first strategy consists in computing the objective function only on the displacement range from zero to the first (either numerical or experimental) fracture point (Fig. 2a), where all load data are available. This option leads to a poor objective function evolution since noise is observed on the surface in Fig. 2a. Moreover this formulation may lead to a wrong solution. In fact from the point of view of the objective function, if the hardening part is well predicted and if the softening part of the curve is short and/or steep, the computed objective function may tend to zero (this specific case is illustrated in the scheme Fig. 2a), leading to a wrong solution.

The second option is to extend the displacement range of the objective function computation to the second fracture point. The missing load data are then replaced by zero load values (Fig. 2b). This option leads to a smooth evolution of the objective function. But this evolution is stiff. This stiffness is due to the large gap which is introduced by the zero load values. This stiffness may be a drawback for the optimization method, especially to build the kriging meta-model. In fact this stiff variation in the objective function cannot be well captured by the kriging meta-model which is more suitable for describing smooth evolutions of the objective function.

Therefore a third option is proposed. The missing load data are replaced by the last recorded load from the experimental test (Fig. 2c). This last option leads to a smooth evolution of the objective function and to a less stiff evolution. This objective function computation will therefore be used in the following.

The reader must keep in mind that these different options do not change the calibration result. These options only impact the shape of the objective function in the research space and consequently the efficiency of the minimization method.

In the next part of this section, calibration results using digital experimental data are presented. First, only 2 damage parameters are considered as unknowns, while all the other parameters are set to their nominal values (Table 1). Secondly, three of them are considered as unknowns in the calibration method.

4.2. Identification of 2 parameters of the damage model: S_0 and $\bar{\varepsilon}_d$

In this section the identification of 2 parameters of the damage model are investigated, respectively S_0 and $\bar{\varepsilon}_d$ (Table 1). In order to evaluate the accuracy of the calibration results, the identification error is defined using the following formula:

$$Error = \frac{|P_i^{N.V.} - P_i^{Id.V.}|}{r_i} \tag{9}$$

where $P_i^{N.V.}$ and $P_i^{Id.V.}$ are respectively the nominal (which is known exactly thanks to the use of digital experimental data) and the identified values of parameter P_i, and r_i is the width of the research range.

The calibration is done using the objective function given in (Eq. (8)). This objective function is minimized thanks to the *EGO* algorithm described in Section 3.2. The research ranges of both parameters are given in Table 2.

After convergence, a value of 0.22% of the objective function is reached. The identified values and the associated errors are given in Table 2. Fig. 3a shows the nominal load-displacement curve and the identified curve.

The calibration results are good for this first test. A very good match between both curves is observed (Fig. 3a), and the calibration errors on both parameters are low. Fig. 3b shows the kriging surface which is obtained after the convergence of the minimization method. This surface exhibits the global minimum located very close to the nominal value (N.V.) point. A local minimum, located at $\bar{\varepsilon}_d = 0.09$ and $S_0 = 1.1$, can also be observed. This first test

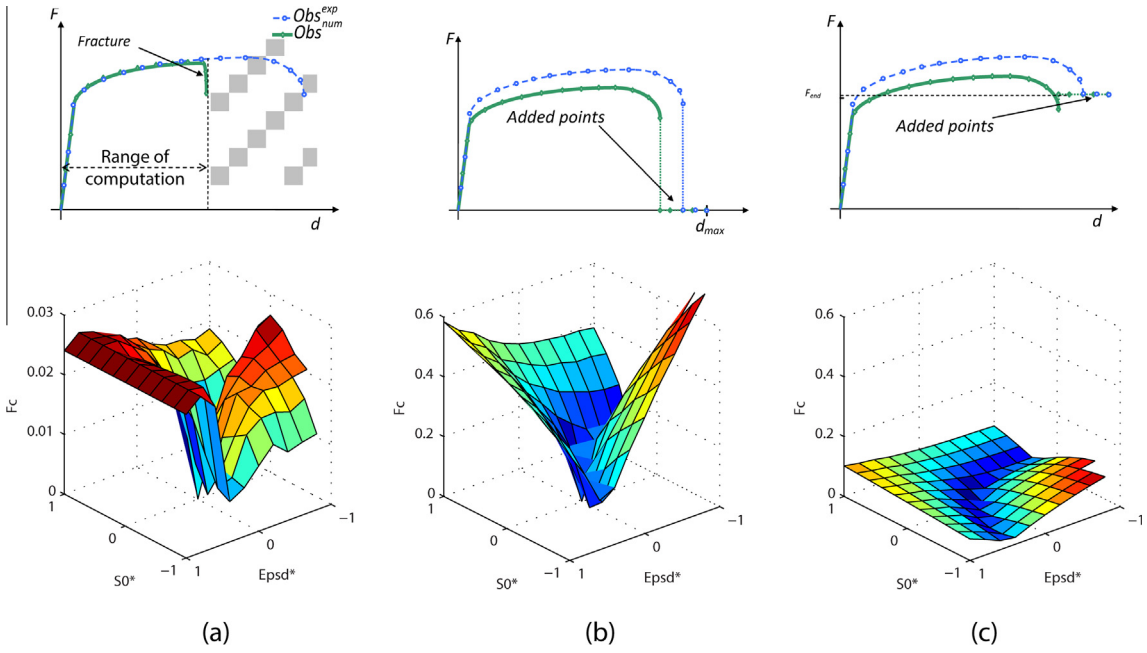

Fig. 2. Three different objective function formulations based on load-displacement measurements – methodology to account for the softening and the fracture parts of the curve.

Table 2
Identification of two parameters – research ranges and results.

Parameters	Nominal value (N.V.)	Research range	Identified value (Id.V.)	Error (%)
b	1	N.V.	–	–
S_0 (MPa)	0.7	[0.1–3]	0.638	2.1
$\bar{\varepsilon}_d$	0.16	[0.04–0.20]	0.163	1.8

shows that if only 2 parameters are calibrated, the method is able to recover the nominal values of the parameters using only global measurements coming from load-displacement data.

4.3. Identification of 3 parameters of the damage model: S_0, $\bar{\varepsilon}_d$ and b

In this section the identification of 3 parameters of the damage model is investigated. The identification includes S_0, $\bar{\varepsilon}_d$ (like in the previous section); but now the parameter b is added to the identification process (Table 1).

The research ranges of all parameters are given in Table 3. After the convergence of the minimization method, the objective function decreases to a value of 0.2%. The identified values and the associated errors are given in Table 3. The result of this calibration is satisfying in term of objective function value. However, parameter b is identified with a large error equals to 15.4%. This test highlights an issue regarding the identification of the b parameter of the Lemaitre damage model.

For calibration problems involving 3 parameters, the kriging meta-model included in the *EGO* algorithm is a 3D function. Displaying this meta-model requires the use of cross-sections. Fig. 4 shows the kriging meta-model obtained after convergence of the minimization method. Fig. 4a (respectively b and c) shows the cross-section of the meta-model for 2 parameters, the third

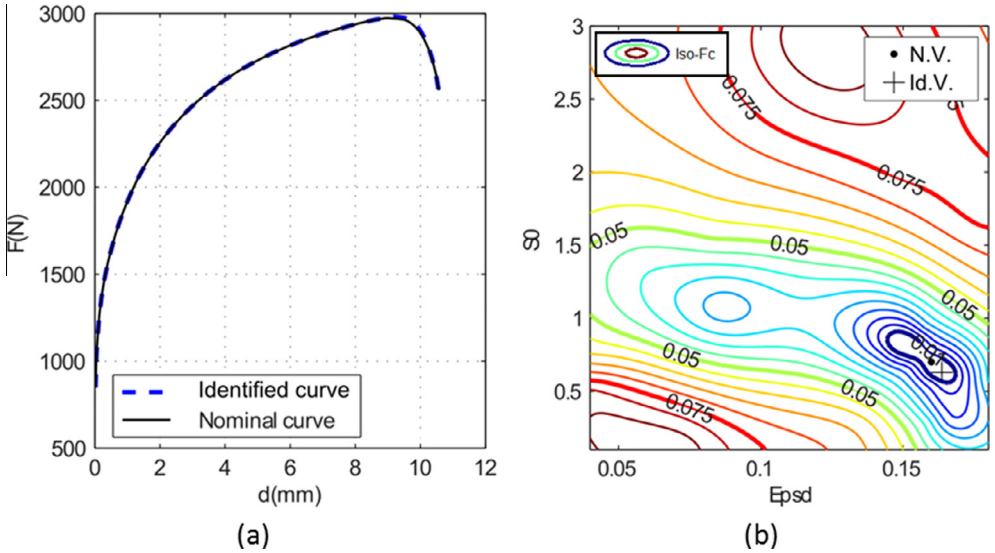

Fig. 3. (a) Load-displacement curve, (b) response surface of the objective function.

Table 3
Identification of three parameters using load-displacement data – research ranges and results.

Parameters	Nominal value (N.V.)	Research range	Identified value	Error (%)
b	1	[0.5–3]	0.61	15.4
S_0 (MPa)	0.7	[0.1–3]	0.78	2.75
$\bar{\varepsilon}_d$	0.16	[0.04–0.20]	0.159	0.75

one S_0 (respectively $\bar{\varepsilon}_d$ and b) is fixed to the identified value to plot the surface.

Cross-sections plotted in Fig. 4a and c show a clear localization of the minimum, whereas the cross-section in Fig. 4b exhibits two minima. For, at least, two values of the b parameter ($b = 0.61$ and $b = 2.4$) the objective function reaches different minima. This graph confirms the issues around the identification of the b parameter.

According to this graph, it is not possible to conclude that the problem exhibits multiple minima or exhibits a weak sensitivity of the b parameter toward the objective function. In fact the two minima observed in Fig. 4b may be due the kriging interpolation method itself. Nevertheless multiple values of b lead to a good value of the objective function. This means that multiple good matching between the nominal load-displacement curve and the identified curve are found.

The information contained in the load-displacement is not rich enough to identify the b parameter value in a unique way. In the next sections additional measurements are added into the calibration process to overcome this issue.

5. Addition of the necking measurement in the calibration process

The softening behavior observed during the tensile test is a combination of two mechanical phenomena: damage growth and necking related to plasticity. Many discussions still take place in the damage mechanics community regarding both phenomena (Morgeneyer et al., 2014): does necking involves localization and void nucleation/growth or does void nucleation/growth induces necking?

In this section the measurements of the tensile specimen necking is added to the objective function in order to increase the amount of experimental information used in the calibration process. These kinds of approaches are often made in the literature (Mahnken, 2002; Munoz-Rojas et al., 2010).

A digital extensometer is used to measure the width reduction of the sample during the tensile test. The necking-displacement curve is recorded. This curve is a 2D curve, therefore the same objective function formulation as in Section 4 (Eq. (8)) is used. Two objective functions are computed: the first one is linked to the load-displacement curve f_F and the second one is linked to the necking-displacement curve f_N. Both functions need to be minimized, therefore a global objective function f_G is computed for the minimization algorithm:

$$f_G = w_F * f_F + w_N * f_N \tag{10}$$

where w_F and w_N are respectively the weights associated to the load-displacement and to the necking objective functions. These parameters are respectively set to 0.8 and 0.2. The identification is done on the three parameters S_0, $\bar{\varepsilon}_d$ and b. The same conditions as in Section 4.3 are used.

Table 4 shows the nominal values, the research ranges and the identified values and their respective error compared to the exact value. After convergence, the objective function decreased to a value of 0.22% ($f_F = 0.17\%$ and $f_N = 0.43\%$). In Fig. 5 the cross-sections of the kriging meta-model are shown.

This calibration, which includes the necking local information, does not improve significantly the identification of parameter b. The error made on parameter b is still large (19.3%). The error is larger than the error found in the previous test (Table 3). The difference can be explained by the fact that the minimization method has converged to another solution. Moreover the valley in the direction of the b parameter is still visible on the kriging cross-section in Fig. 5a and b. It must be noticed that the local minimum observed when only the load-displacement curve is used (Fig. 4b, $b = 2.5$) disappears when necking local information is added in the objective function. Indeed no local minimum can be observed anymore at $b = 2.5$ in Fig. 5b. This slight improvement is therefore a motivation to add richer data into the calibration process.

During the minimization process, several set of parameters are tested. In Fig. 6 all these sets are displayed. On each graph, for each set of parameters one blue point is plotted. On the x-axis one can read the objective function value, and on the y-axis one can read the value of the parameters of the set. Fig. 6a presents the $\bar{\varepsilon}_d$ values in function of the objective function values. One can easily see a clear convergence toward the nominal value of 0.16. The same behavior is observed in Fig. 6b for the S_0 parameter, a convergence toward the nominal value of 0.7 is observed. In Fig. 6c the behavior is not the same; the b parameter converges towards multiple minima. This graph highlights again the issue regarding the unicity of the b parameter identification.

6. Integration of full field measurements in the calibration process

In this last part, richer data are added in the calibration process using full field measurements. The full field measurements method allows obtaining local evolution of kinematic fields during the mechanical test. These additional data are extremely useful to improve material behavior analysis a material behavior and to calibrate models (Grediac and Hild, 2011; Ienny et al., 2009).

In this work the displacement field is used to compute the objective function. Some authors make the choice of working with strain measurements instead of displacement (Lecompte et al., 2007). This choice is relevant when localization of strains does not occur. When strain localization is observed (as in ductile fracture) working with displacement is more robust.

In the proposed approach displacement field at the surface of the sample is used. The used displacement fields are comparable to measurements coming from 2D-DIC method, the third component of the displacement field is not taken into account.

Displacement fields are used both to compute an extra objective function and to define the appropriate boundary conditions of the FE model. Many ways of incorporating full field measurements in inverse approaches can be found in the literature. An overview of all these solutions can be found in (Ienny et al., 2009).

6.1. Objective function based on full displacement field within a larger deformation framework

In order to use a full field measurement approach for ductile damage parameters identification, the framework must be adapted to large deformation. In fact, during the calibration process, several damage parameter values are tested. Therefore the final shape of the FE sample is not the same as the final shape of the experimental sample (except when the convergence is reached). The localization of strains and the failure locations may be different. In order to compute a relevant objective function, the kinematic fields coming from the experiment and from the FE model must be expressed in a comparable base. Springmann and Kuna (2006) overcame this

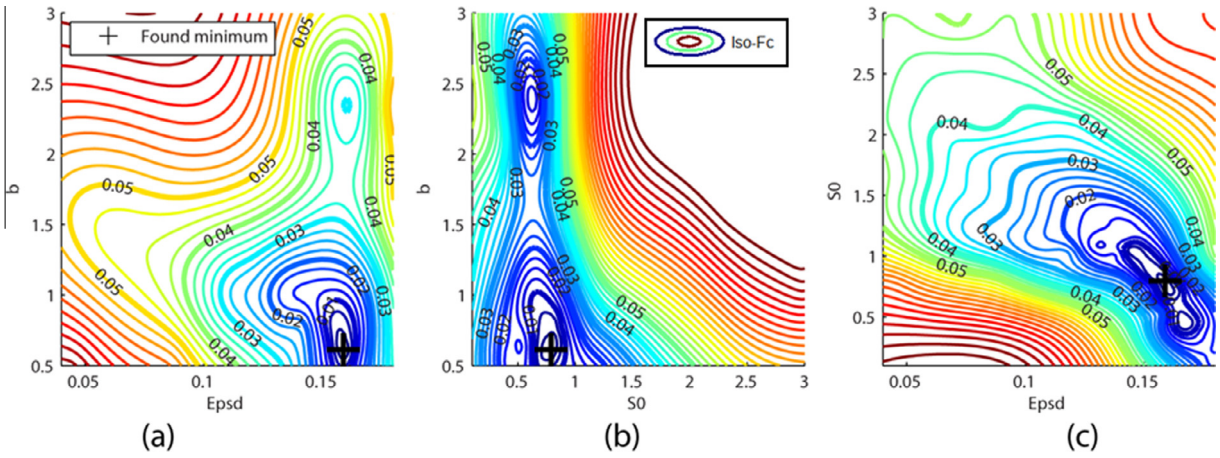

Fig. 4. Identification of three parameters using load-displacement data - response surfaces of the objective function – cross sections (a) b vs. $\bar{\varepsilon}_d$, (b) b vs. S_0, (c) S_0 vs. $\bar{\varepsilon}_d$.

Table 4
Identification of three parameters using load-displacement curve and necking-displacement curve – research ranges and results.

Parameters	Nominal value (N.V.)	Research range	Identified value	Error (%)
b	1	[0.5–3]	0.51	19.6
S_0 [MPa]	0.7	[0.1–3]	0.706	0.23
$\bar{\varepsilon}_d$	0.16	[0.04–0.20]	0.161	0.6

issue using a coincident mesh at the surface of the specimen between the measurement and the FE model. Therefore an objective function for the trajectories of each material point (node of the mesh) can be computed, and next a sum all over the nodes leads to the full field objective function. This approach is efficient, but the use of coincident mesh has some limitations: the use of finer mesh or of re-meshing is not possible.

An approach which allows more freedom in the mesh definition is presented in this section. The main idea of the approach is to express all the kinematic fields in the non-deformed configuration; then these fields are projected on the same base (the same grid) in order to evaluate the objective function.

First, full field digital experimental data must be synthetized. The displacement fields of the surface of the sample coming from the digital experimental FE model are projected on a regular grid. In Fig. 7a and b, the in-plane components of the displacement fields are shown (Ux^{exp} and Uy^{exp}), the third component is not measured. Fig. 7c shows the validity indicator of the measurements; this indicator δ_i is equal to one if the measurement is available, and is equal to zero if not (i.e. if the measurement point is outside the sample). This procedure is done for each time increment. It finally leads to obtain T snap-shoots of the displacement field.

The same kind of grid can be obtained from digital image correlation method based on real measurements.

Secondly the numerical displacement field of the surface of the sample is extracted from the FE simulation (Fig. 7d). At this point numerical and experimental data are expressed on different meshes and the shape of each sample is different. In order to build a relevant objective function the same material points must be compared. The choice is made to express all the fields in the undeformed configuration, therefore the lagrangian displacement of each mesh is used to jump back to the initial configuration, where the samples have the same shape by definition. The numerical displacement field is then interpolated on the regular grid of the experimental measurements. These different steps are described in the flowchart in Fig. 8. After this treatment, experimental and numerical data of the same material point are available on the same node of the grid; the objective function can be now easily computed.

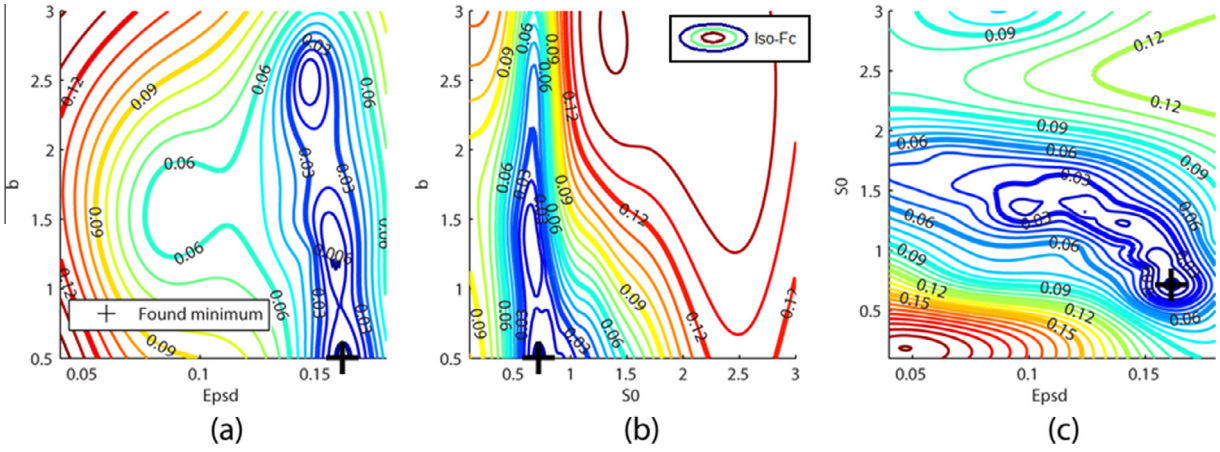

Fig. 5. Identification of three parameters using load-displacement curve and necking-displacement curve - response surfaces of the objective function – cross sections (a) b vs. $\bar{\varepsilon}_d$, (b) b vs. S_0, (c) S_0 vs. $\bar{\varepsilon}_d$.

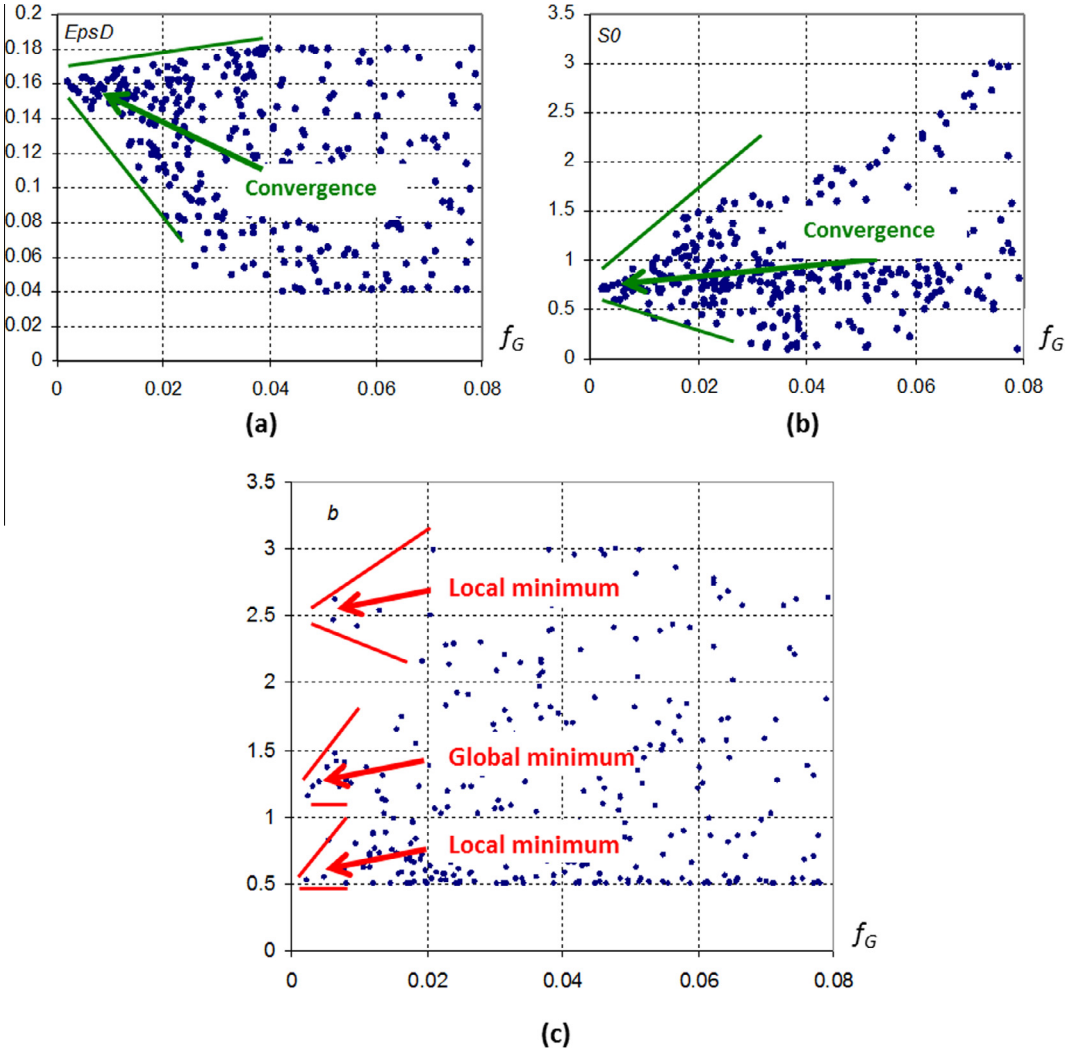

Fig. 6. Scattering of the parameters value during the minimization process (a) $\bar{\varepsilon}_d$, (b) S_0, (c) b.

The objective function is based on the generic formula (Eq. (6)), and is expressed for each component of the displacement field:

$$f_{DF,j}(P) = \sum_{t=1}^{T}\left(\sqrt{\frac{\sum_{i=1}^{n}\left[\delta_{i,t}\left(Uj_{i,t}^{num}(P) - Uj_{i,t}^{\exp}\right)\right]^2}{\sum_{i=1}^{n}\left[\delta_{i,t}Uj_{i,t}^{\exp}\right]^2}}\right) \tag{11}$$

where j is equal to x or y, and $\delta_{i,t} = \max(\delta_{i,t}^{num}, \delta_{i,t}^{\exp})$, $\delta_{i,t}^{\exp}$ (respectively $\delta_{i,t}^{num}$) validity indicator of the measurements for the experimental measurement (respectively the numerical measurements) for each node i and for each time increment t. This objective function is based on the sum of squared difference of the displacement (numerical and experimental) over the n nodes of the grid and over the time increments.Both components of the objective function are then added to obtain a scalar objective function which is representative of the gap between the numerical and the experimental displacement fields:

$$f_{DF}(P) = \omega_x f_{DF,x}(P) + \omega_y f_{DF,y}(P) \tag{12}$$

where ω_x and ω_y are the weights of each objective function.

Like for the load-displacement curve, it may occur that data are not available at few points (in case of earlier fracture of one of the sample). Therefore the same approach as in Section 4.1 is applied. The missing data are replaced by the last available data at the current point:

$$\begin{aligned} &\text{if } \delta_{i,t}^{num} = 0, \text{ then } \begin{cases} Ux_{i,t}^{num} = Ux_{i,t-1}^{num} \\ Uy_{i,t}^{num} = Uy_{i,t-1}^{num} \end{cases} \\ &\text{if } \delta_{i,t}^{\exp} = 0, \text{ then } \begin{cases} Ux_{i,t}^{\exp} = Ux_{i,t-1}^{\exp} \\ Uy_{i,t}^{\exp} = Uy_{i,t-1}^{\exp} \end{cases} \end{aligned} \tag{13}$$

With the approach described in this section, an objective function based on the displacement field can be computed. In order to discriminate solutions and to make the minimization faster, the information coming from the load-displacement curve is used as well in the global objective function. A weighted sum is used:

$$f_G(P) = \omega_x f_{DF,x}(P) + \omega_y f_{DF,y}(P) + \omega_F f_F(P) \tag{14}$$

Since each objective function is normalized (Eqs. (8) and (11)) all the weights are set to the same value: $\omega_x = \omega_y = \omega_F = 1/3$. It must be noticed that the objective function based on the necking measurements is not used (Section 5) in (Eq. (14)). Indeed the necking information is embedded in the objective function $f_{DF,x}(P)$.

The proposed approach is described for 2D displacement fields but can be easily extended to 3D measurements.

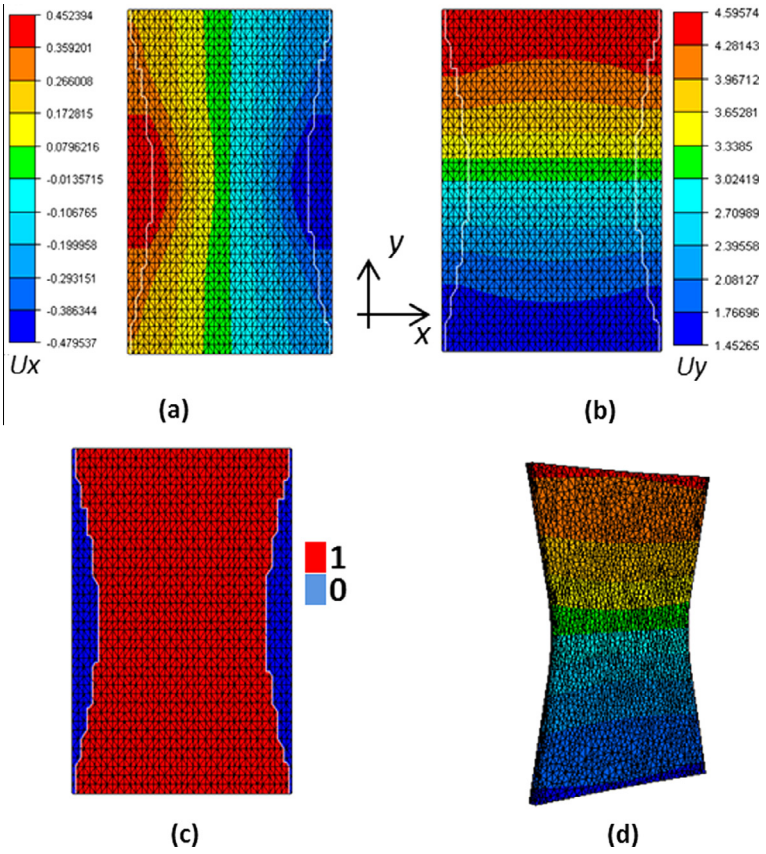

Fig. 7. Synthetic full field measurements data – (a) and (b) components of displacement field, (c) validity data indicator, (d) view of the 3D FE mesh.

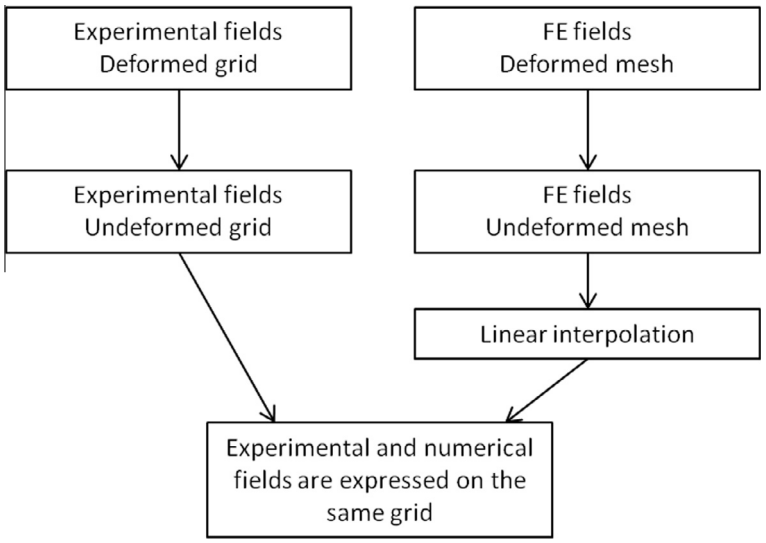

Fig. 8. Flowchart of the mapping method of the displacement fields between experimental en FE measurements in a large deformation framework.

6.2. Calibration results based on full displacement field measurements

The global objective function (Eq. (14)) is minimized using the EGO algorithm. Table 5 shows the nominal values, the research ranges, the identified values and their respective errors compared to the exact value after convergence of the minimization method. Fig. 9 shows the cross-section of the kriging meta-model after convergence. Each column represents the kriging response surface of the components of the objective function, respectively from left to right: the objective function linked with the load $f_F(P)$, the objective function linked with the x component of the displacement $f_{DF,x}(P)$, the objective function linked with the y component of the displacement, and the global objective function $f_G(P)$ (Eq. (14)). Each line represents the kriging response surface for a couple of parameters, respectively from top to bottom: (b, S_0), $(S_0, \bar{\varepsilon}_d)$, and $(b, \bar{\varepsilon}_d)$.

Results presented in Fig. 9 and Table 5 allow making several remarks on the interest of using full field measurements:

Table 5
Identification of three parameters using load-displacement curve and full displacement field measurements – research ranges and results.

Parameters	Nominal value (N.V.)	Research range	Identified value	Error (%)
b	1	[0.5–3]	0.856	5.7
S_0 [MPa]	0.7	[0.1–1.5]	0.703	0.21
$\bar{\varepsilon}_d$	0.16	[0.04–0.20]	0.153	0.44

- Sensitivity toward the couple of parameters (b, S_0) (Fig. 9, line 1):
  - The local minimum at b = 2.5 and S_0 = 0.7 MPa (Fig. 9, line 1, column 1) on the force objective function ($f_F(P)$) is canceled out thanks to the objective function linked with the x component (Fig. 9, line 1, column 2). This observation is in agreement with remarks done about the necking objective function (Section 5). Indeed necking measurement is embedded in the x component of the displacement.
  - The global objective function (Fig. 9, line 1, column 4) still exhibits multiple minima. It must be noticed that other choice of weighting parameters in (Eq. (14)) could improve this point. In particular, it can be seen that the cost function associated with Ux tends to eliminate the higher values of parameter b.
- Sensitivity toward the couple of parameters (S_0, $\bar{\varepsilon}_d$) (Fig. 9, line 2): the force kriging surface (Fig. 9, line 2, column 1) exhibits a valley, which is the signature of a correlation between parameters. But this valley is no more visible on displacement field objective functions (Fig. 9, line 2, column 2 and 3). Full field objective functions are therefore efficient to suppress the correlation between the S_0 and the $\bar{\varepsilon}_d$ parameters.
- Sensitivity toward the couple of parameters (b, $\bar{\varepsilon}_d$) (Fig. 9, line 3): the shape of the three surfaces is very close; no clear improvement can be seen for this couple of parameters. It must be noticed here that the local minimum observed for $b \sim 2.5$ in the first line of Fig. 9 is not a minimum anymore here.

This sensitivity analysis on the full field objective function shows that using displacement field measurements resolve some issues regarding damage parameters identification. The transverse displacement field (component x) improves slightly the sensitivity toward the b parameter. And both components of the displacement fields allow removing the correlation between (S_0, $\bar{\varepsilon}_d$). Parameter b still exhibits calibration difficulties within the range of [0.5 1.1] (weak sensibility and multiple local minima, as already exhibited in Fig. 5(a) and (b) and Fig. 6). This means that the new surface displacement observables are not rich enough to significantly improve the calibration of the b parameter. The use of out-of-plane displacements would be necessary here to overcome this non-unique solution.

7. Conclusion

The present work deals with a methodology to identify the Lemaitre damage model parameters. An inverse analysis approach based on a tensile test is studied here. Several kinds of

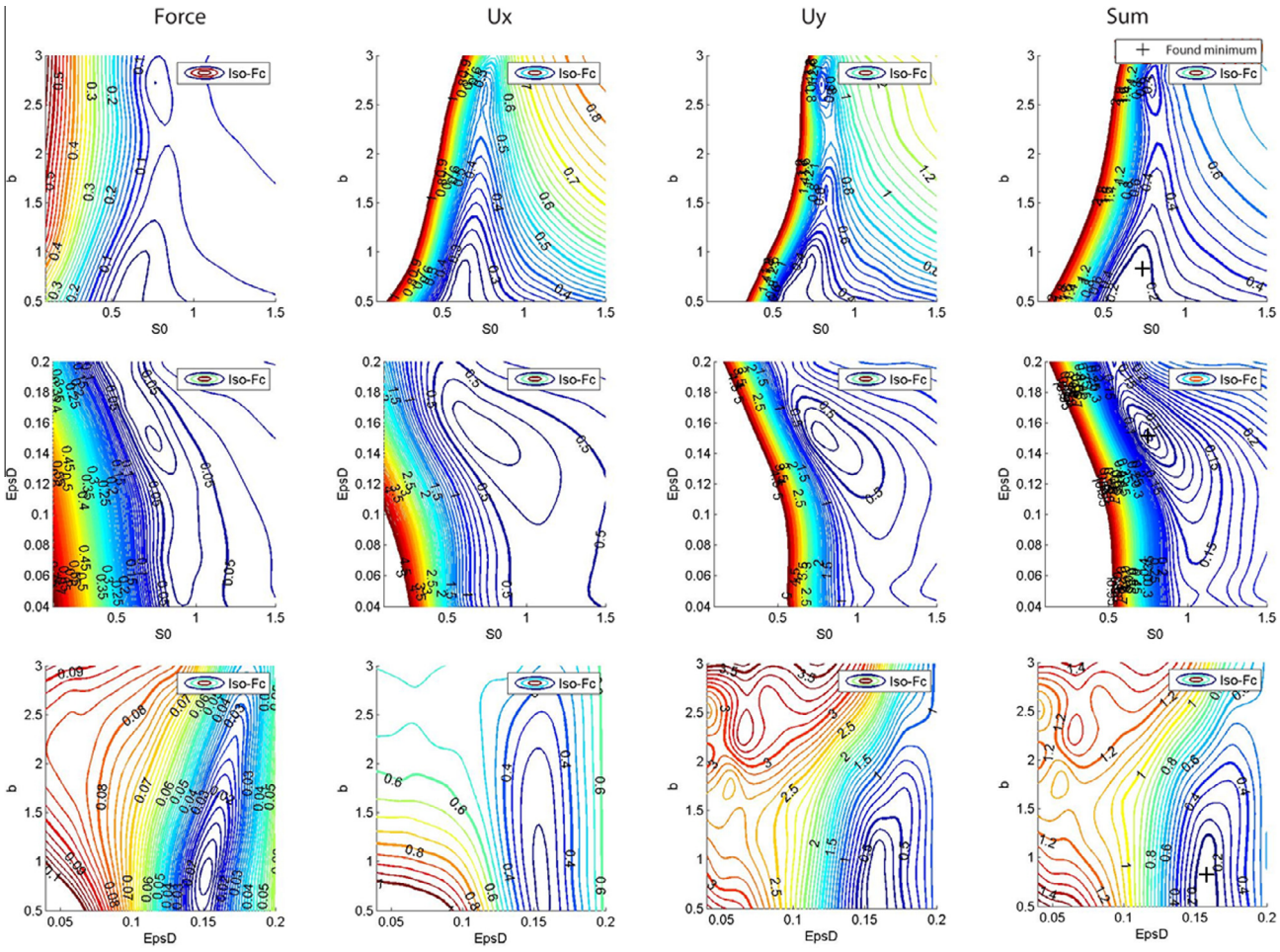

Fig. 9. Identification of three parameters using displacement field data and load-displacement data – response surfaces of the objective function.

measurements are introduced in the calibration process step by step. First the load-displacement curve is exploited, then necking measurements are introduced in the calibration process, and finally displacement full field measurements are used. For each kind of measurements an adapted formulation of the objective function is proposed. These formulations are adapted to catch in a relevant way the softening part of the material behavior which is impacted by ductile damage.

In order to analyze only the damage parameters identification, numerical data are used as "experimental" measurements. This avoids any kind of uncertainty related to numerical issues and to the plastic behavior of the material.

The minimization of the objective function is done by a minimization algorithm assisted by meta-model (the *EGO* algorithm). Results are analyzed using response surfaces coming from the meta-model which is built during the minimization process. These surfaces are a powerful tool since it allows detecting weak sensitivity effects, correlation between parameters and multiple minima issues.

The first step, based on the load-displacement curve, shows that the value of the Lemaitre model parameter b cannot be identified accurately. The load-displacement curve is a global observable that is not rich enough to ensure the uniqueness of the parameter identification. Then necking measurements are added in the calibration process and the sensitivity of the b parameter is slightly enhanced thanks to this additional local measurement. This improvement is also noticed when full field measurements are used to compute the objective function. The use of full field measurements and especially of the transverse displacement field is a good way to resolve partially the issue of the identification of the b parameter of the Lemaitre damage model. Moreover, full field measurements are very efficient to suppress the correlation between damage parameters, which was observed when only the load-displacement curve was considered.

Future works are to apply this approach to a real data. To achieve this goal the plastic behavior of the material should be well described to reproduce the kinematic fields before damage occurs. The same methodology to calibrate the full constitutive model (elastic-plastic coupled to damage) is very promising. Identifying hardening and damage parameters requires the use of global and local information. Two enhancements of the procedure may improve the efficiency and the accuracy of the calibration according to the authors:

- Extension of the methodology to full 3D measurements of displacement fields at the surface or in the thickness.
- Calibration on multiple tests, involving different stress states.

Identification of the b parameter may be improved by using these enhancements. The knowledge of the localized necking combined with a different test, with a different stress state (shear test for example), will undoubtedly enrich the observable basis and may increase the sensitivity of the b parameter.

Moreover the methodology can be extended to take into account even richer information as volumetric measurements coming from digital volume correlation (Morgeneyer et al., 2014; Roux et al., 2008). A first step in this direction has been done by Cao et al. (2014) where void volume fraction measurements coming from X-ray micro-tomography are introduced in the calibration procedure.

Acknowledgement

The authors wish to thank CETIM for their financial support within the project Mona Lisa.

References

Abbasi, M., Ketabchi, M., Izadkhah, H., Fatmehsaria, D.H., Aghbash, A.N., 2011. Identification of gtn model parameters by application of response surface methodology. Proc. Eng. 10, 415–420. http://dx.doi.org/10.1016/j.proeng.2011.04.070.

Abbassi, F., Belhadj, T., Mistou, S., Zghal, A., 2013. Parameter identification of a mechanical ductile damage using artificial neural networks in sheet metal forming. Mater. Design 45, 605–615. http://dx.doi.org/10.1016/j.matdes.2012.09.032.

Bai, Y., Wierzbicki, T., 2008. A new model of metal plasticity and fracture with pressure and lode dependence. Int. J. Plast. 24 (6), 1071–1096. http://dx.doi.org/10.1016/j.ijplas.2007.09.004.

Bouchard, P.-O., Laurent, T., Tollier, L., 2008. Numerical modeling of self-pierce rivetingfrom riveting process modeling down to structural analysis. J. Mater. Process. Technol. 202 (1–3), 290–300. http://dx.doi.org/10.1016/j.jmatprotec.2007.08.077.

Bouchard, P.-O., Bourgeon, L., Fayolle, S., Mocellin, K., 2011. An enhanced lemaitre model formulation for materials processing damage computation. Int. J. Mater. Forming 4 (3), 299–315. http://dx.doi.org/10.1007/s12289-010-0996-5.

Bouterf, A., Roux, S., Hild, F., Vivier, G., Brajer, X., Maire, E., Meille, S., 2014. Damage law identification from full field displacement measurement: Application to four-point bending test for plasterboard. Eur. J. Mech. A/Solids. http://dx.doi.org/10.1016/j.euromechsol.2014.06.001.

Bridgman, P., 1944. The stress distribution at the neck of a tension specimen. Trans. ASM 32, 553–574.

Broggiato, G.B., Campana, F., Cortese, L., 2007. Identification of material damage model parameters: an inverse approach using digital image processing. Meccanica 42 (1), 9–17. http://dx.doi.org/10.1007/s11012-006-9019-5.

Cao, T.-S., Gaillac, A., Montmitonnet, P., Bouchard, P.-O., 2013. Identification methodology and comparison of phenomenological ductile damage models via hybrid numerical-experimental analysis of fracture experiments conducted on a zirconium alloy. Int. J. Solids Struct. 50 (24), 3984–3999. http://dx.doi.org/10.1016/j.ijsolstr.2013.08.011.

Cao, T.-S., Maire, E., Verdu, C., Bobadilla, C., Lasne, P., Montmitonnet, P., Bouchard, P.-O., 2014. Characterization of ductile damage for a high carbon steel using 3d x-ray micro-tomography and mechanical tests application to the identification of a shear modified gtn model. Comput. Mater. Sci. 84, 175–187. http://dx.doi.org/10.1016/j.commatsci.2013.12.006.

Chen, W.H., 1971. Necking of a bar. Int. J. Solids Struct. 7 (7), 685–717. http://dx.doi.org/10.1016/0020-7683(71)90088-6.

Dunand, M., Mohr, D., 2010. Hybrid experimental–numerical analysis of basic ductile fracture experiments for sheet metals. Int. J. Solids Struct. 47 (9), 1130–1143. http://dx.doi.org/10.1016/j.ijsolstr.2009.12.011.

El Khaoulani, R., Bouchard, P.-O., 2012. An anisotropic mesh adaptation strategy for damage and failure in ductile materials. Finite Elem. Anal. Des. 59, 1–10. http://dx.doi.org/10.1016/j.finel.2012.04.006.

El Khaoulani, R., Bouchard, P.-O., 2013. Efficient numerical integration of an elastic plastic damage law within a mixed velocity pressure formulation. Math. Comput. Simul. 94, 145–158. http://dx.doi.org/10.1016/j.matcom.2013.06.004.

Fratini, L., Lombardo, A., Micari, F., 1996. Material characterization for the prediction of ductile fracture occurrence: An inverse approach. J. Mater. Process. Technol. 60 (1–4), 311–316. http://dx.doi.org/10.1016/0924-0136(96)02347-3.

Ginsbourger, D., Riche, R., Carraro, L., 2010. Kriging is Well-Suited to Parallelize Optimization. Adaptation, Learning, and Optimization, vol. 2. Springer, Berlin Heidelberg, pp. 131–162. http://dx.doi.org/10.1007/978-3-642-10701-6_6, Chapter 6, ISBN 978-3-642-10701-6.

Grediac, M., Hild, F., 2011. Mesures de champs et identification en mécanique des solides. Série matériaux et métallurgie, MIM. Hermès-Lavoisier.

Guo, J., Zhao, S., Ri-ichi, M., Zang, S., 2013. Experimental and numerical investigation for ductile fracture of al-alloy 5052 using modified rousselier model. Comput. Mater. Sci. 71, 115–123. http://dx.doi.org/10.1016/j.commatsci.2013.01.011.

Gurson, A.L., 1977. Continuum theory of ductile rupture by void nucleation and growth: Part I criteria and flow rules for porous ductile media. J. Eng. Mater. Technol. 99 (1), 2. http://dx.doi.org/10.1115/1.3443401.

Ienny, P., Caro-Bretelle, A.-S., Pagnacco, E., 2009. Identification from measurements of mechanical fields by finite element model updating strategies. a review. Revue européenne de mécanique numérique, 1779-7179 18 (3-4), 353–376. http://dx.doi.org/10.3166/ejcm.18.353-376.

Jones, D.R., Schonlau, M., Welch, W.J., 1998. Efficient global optimization of expensive black-box function. J. Global Optim. 13, 455–492. http://dx.doi.org/10.1023/A:1008306431147.

Kim, J.H., Serpantié, A., Barlat, F., Pierron, F., Lee, M.-G., 2013. Characterization of the post-necking strain hardening behavior using the virtual fields method. Exp. Mech. 50 (24), 3829–3842. http://dx.doi.org/10.1016/j.ijsolstr.2013.07.018.

Kim, J.H., Barlat, F., Pierron, F., Lee, M.-G., 2014. Determination of anisotropic plastic constitutive parameters using the virtual fields method. Exp. Mech. 54 (7), 1189–1204. http://dx.doi.org/10.1007/s11340-014-9879-x.

Ladevèze, P., Lamaitre, J., 1984. Damage effective stress in quasi unilateral conditions. Int. Congress Theor. Appl. Mech.

Lecompte, D., Smits, A., Sol, H., Vantomme, J., Van Hemelrijck, D., 2007. Mixed numerical–experimental technique for orthotropic parameter identification using biaxial tensile tests on cruciform specimens. Int. J. Solids Struct. 44 (5), 1643–1656. http://dx.doi.org/10.1016/j.ijsolstr.2006.06.050.

Lemaitre, J., 1992. A Course on Damage Mechanics. Springer, Berlin.

Lemaitre, J., Desmorat, R., 2005. Background on Continuum Damage Mechanics. Springer, Berlin Heidelberg, ISBN 978-3-540-27293-9. http://dx.doi.org/10.1007/3-540-27293-3_1.

Mahnken, R., 2002. Theoretical, numerical and identification aspects of a new model class for ductile damage. Int. J. Plast. 18 (7), 801–831. http://dx.doi.org/10.1016/s0749-6419(00)00105-4.

Morgeneyer, T.F., Taillandier-Thomas, T., Helfen, L., Baumbach, T., Sinclair, L., Roux, S., Hild, F., 2014. In situ 3-d observation of early strain localization during failure of thin al alloy (2198) sheet. Acta Materialia 69, 78–91. http://dx.doi.org/10.1016/j.actamat.2014.01.033.

Munoz-Rojas, P.A., Cardoso, E.L., Vaz, M., 2010. Parameter identification of damage models using genetic algorithms. Exp. Mech. 50 (5), 627–634. http://dx.doi.org/10.1007/s11340-009-9321-y.

Périé, J.N., Leclerc, H., Roux, S., Hild, F., 2009. Digital image correlation and biaxial test on composite material for anisotropic damage law identification. Int. J. Solids Struct. 46 (11–12), 2388–2396. http://dx.doi.org/10.1016/j.ijsolstr.2009.01.025.

Pottier, T., Vacher, P., Toussaint, F., Louche, H., Coudert, T., 2012. Out-of-plane testing procedure for inverse identification purpose: application in sheet metal plasticity. Exp. Mech. 52 (7), 951–963. http://dx.doi.org/10.1007/s11340-011-9555-3.

Rousselier, G., 1987. Ductile fracture models and their potential in local approach of fracture. Nuclear Eng. Des. 105 (1), 97–111. http://dx.doi.org/10.1016/0029-5493(87)90234-2.

Roux, E., Bouchard, P.O., 2013. Kriging metamodel global optimization of clinching joining processes accounting for ductile damage. J. Mater. Process. Technol. 213 (7), 1038–1047. http://dx.doi.org/10.1016/j.jmatprotec.2013.01.018.

Roux, S., Hild, F., Viot, P., Bernard, D., 2008. Three-dimensional image correlation from X-ray computed tomography of solid foam. Composites Part A: Appl. Sci. Manuf. 39 (8), 1253–1265. http://dx.doi.org/10.1016/j.compositesa.2007.11.011.

Springmann, M., Kuna, M., 2006. Determination of ductile damage parameters by local deformation fields: Measurement and simulation. Arch. Appl. Mech. 75 (10–12), 775–797. http://dx.doi.org/10.1007/s00419-006-0033-9.

Tardif, N., Kyriakides, S., 2012. Determination of anisotropy and material hardening for aluminum sheet metal. Int. J. Solids Struct. 49 (25), 3496–3506. http://dx.doi.org/10.1016/j.ijsolstr.2012.01.011.

Tvergaard, V., Needleman, A., 1984. Analysis of the cup-cone fracture in a round tensile bar. Acta Metall. 32 (1), 157–169. http://dx.doi.org/10.1016/0001-6160(84)90213-x.

Wagoner, R.H., Chenot, J.L., 2001. Metal Forming Analysis. Cambridge University Press.